ACS OMEGA

http://pubs.acs.org/journal/acsodf

Article

Organorhodium(III)- and Iridium(III)-Substituted 20-Tungstobismuthates(III) and -Antimonates(III), $[(MCp^*)_2X_2W_{20}O_{70}]^{10-}$ (M = Rh^{III} and Ir^{III}; X = Bi^{III} and Sb^{III})

Ali S. Mougharbel, Sihana Ahmedi, Saurav Bhattacharya, Ananthu Rajan, and Ulrich Kortz*

Cite This: *ACS Omega* 2021, 6, 34494−34500

Read Online

ACCESS | Metrics & More | Article Recommendations | Supporting Information

ABSTRACT: The synthesis of four organometallic RhCp*- and IrCp*-containing heteropoly-20-tungstates, $[\{RhCp^*\}_2Bi_2W_{20}O_{70}]^{10-}$ (**1**), $[\{IrCp^*\}_2Bi_2W_{20}O_{70}]^{10-}$ (**2**), $[\{RhCp^*\}_2Sb_2W_{20}O_{70}]^{10-}$ (**3**), and $[\{IrCp^*\}_2Sb_2W_{20}O_{70}]^{10-}$ (**4**) has been accomplished by reaction of $(MCp^*Cl_2)_2$ with $[X_2W_{22}O_{74}(OH)_2]^{12-}$ in aqueous solution at pH 6 and 70 °C. The four polyanions **1**−**4** were structurally characterized in the solid state by single-crystal XRD, FTIR, and TGA and in solution by ^{183}W and ^{13}C NMR. For the Rh derivatives **1** and **3** the $^{183}W-^{103}Rh$ coupling ($^2J_{W\text{-}Rh}$ 3.0 Hz) could be identified by ^{183}W NMR.

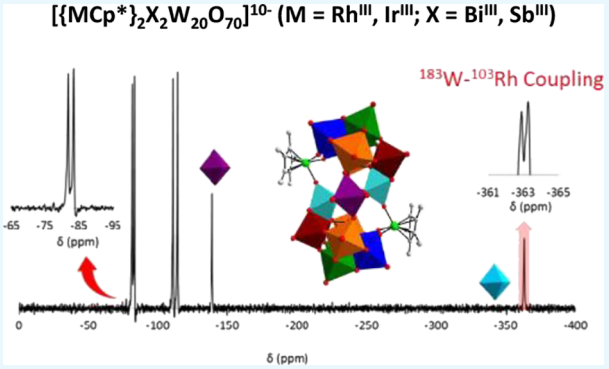

INTRODUCTION

Polyoxometalates (POMs) constitute a unique class of anionic metal-oxo clusters, which can be formed by acidification of aqueous solutions of simple oxometallate ions (e.g., WO_4^{2-} and MoO_4^{2-}) and possibly a hetero group (e.g., phosphate, silicate, and germanate).[1] POMs with a wide variety of shapes, sizes, and compositions can be obtained by simply tuning the reaction parameters, such as pH, temperature, stoichiometric ratio and concentration of reagents, as well as ionic strength.[2] Noble metal-containing POMs are of particular interest for catalytic applications.[3] The reactivity of rhodium and iridium ions with POMs, including organometallic derivatives such as $Rh^{III}Cp^*$ and $Ir^{III}Cp^*$ ($Cp^* = C_5Me_5$), is an attractive research area. In 1984, Klemperer reported the organorhodium-capped mixed-metal Lindqvist derivative $[(Cp^*Rh)Nb_2W_4O_{19}]^{2-}$,[4a] and in the same year Finke and Droege reported with a dicationic $(Rh^{III}Cp^*)^{2+}$ group covalently grafted to a $[SiW_9Nb_3O_{40}]^{7-}$ Keggin ion via three bridging oxygens of a NbW_2O_{13} triad,[4b] and this work was followed up by Nomiya et al.[5] In 1993, Gouzerh and co-workers reported on five lacunary Lindqvist-type polyanions having $Rh^{III}Cp^*$ groups grafted, such as $[Mo_5O_{13}(OCH_3)_4(NO)\{RhCp^*(solv)\}]^-$ (solv = H_2O and MeOH) and $[Mo_5O_{13}(OCH_3)_4(NO)\{(RhCp^*)_2(\mu\text{-}X)\}]$ (X = Cl and Br).[6] In 2000, Nomiya and Hasegawa reported the Wells−Dawson ion with two $Rh^{III}Cp^*$ groups grafted, $[(Cp^*Rh)_2P_2W_{15}V_3O_{62}]^{5-}$,[7] and in the following year the same authors reported the Keggin derivative $[(Cp^*Rh)PW_9V_3O_{40}]^{4-}$.[8] In 2002, Nomiya et al. also reported the Wells−Dawson derivative $[(Cp^*Rh)P_2W_{16}V_2O_{62}]^{6-}$.[9] In 2003, Isobe and co-workers reported the first Cp*Rh-capped triple cubane- and windmill-type isomers, $[(Cp^*Rh)_4W_4O_{16}]$.[10] In 2015, Nomiya and co-workers introduced a dimeric tri-titanium(IV)-substituted Wells−Dawson ion with two bridging $[RhCp^*]^{2+}$ groups, $[(Cp^*Rh)_2(Ti_3P_2W_{15}O_{60}(OH)_2)_2]^{16-}$.[11] In the same year, the Lindqvist-type tantalate ion $[trans\text{-}(Cp^*Rh)_2Ta_6O_{19}]^{4-}$ was reported by Abramov et al.[12] In 2017, Wang and co-workers reported on the Cp*Rh-grafted molybdophosphates $[(Cp^*Rh)_4PMo_8O_{32}]^{3-}$ and $[Na_2(Cp^*Ir)_4PMo_8O_{34}]^{5-}$,[13] and in the following year, they prepared the octatungstate $[(Cp^*M)_4W_8O_{32}]^{8-}$ (M = Rh and Ir).[14] Overall, the number of IrCp*-containing POMs is smaller than those containing RhCp*. In 2016, Abramov et al. reported on the hexaniobate dimer $[H_2\{Cp^*Ir\}_2(Nb_6O_{18})_2O]^{8-}$ and the hexatantalates $[(Cp^*Ir)Ta_6O_{19}]^{6-}$ and $[(Cp^*Ir)_2Ta_6O_{19}]^{4-}$.[15] Herein, we report on the reactivity of RhCp* and IrCp* with the heteropoly-22-tungstates $[X_2W_{22}O_{74}(OH)_2]^{12-}$ (X = Sb^{III} and Bi^{III}).

EXPERIMENTAL SECTION

Materials and Methods. Rhodium(III) chloride hydrate ($RhCl_3{\cdot}xH_2O$), iridium(III) chloride hydrate ($IrCl_3{\cdot}xH_2O$),

Received: August 28, 2021
Accepted: November 15, 2021
Published: December 8, 2021

Table 1. Crystal Data and Structure Refinement of NaK-1, Na-2, NaK-3, and Na-4

compound	NaK-1	Na-2	NaK-3	Na-4
empirical formula[a]	$KNa_4Rh_2C_{20}Bi_2W_{20}H_{30}O_{94}$ ($KNa_9Rh_2C_{20}Bi_2W_{20}H_{98}O_{104}$)	$Na_5Ir_2C_{20}Bi_2$ $W_{20}H_{30}O_{87}$ ($Na_{10}Ir_2C_{20}Bi_2W_{20}H_{140}O_{125}$)	$K_2Na_3Rh_2C_{20}Sb_2W_{20}H_{30}O_{96}$ ($K_5Na_5Rh_2C_{20}Sb_2W_{20}H_{98}O_{104}$)	$Na_{3.5}Ir_2C_{20}Sb_2W_{20}H_{30}O_{89}$ ($Na_{10}Ir_2C_{20}Sb_2W_{20}H_{130}O_{100}$)
formula weight (g/mol)[a]	6206.3 (6550.0)	6256.8 (7090.0)	6079.9 (6439.5)	6079.8 (6986.0)
crystal system	triclinic	triclinic	triclinic	triclinic
space group	$P\bar{1}$	$P\bar{1}$	$P\bar{1}$	$P\bar{1}$
a (Å)	13.6643(11)	17.1496(17)	13.6825(7)	17.1405(19)
b (Å)	13.7610(11)	19.521(2)	13.7623(7)	19.507(2)
c (Å)	18.2754(14)	23.720(3)	18.3248(10)	23.730(3)
α (°)	72.177(2)	103.050(3)	72.603(2)	103.028(3)
ß (°)	84.281(2)	99.932(3)	83.896(2)	100.372(3)
γ (°)	88.693(2)	113.932(3)	89.231(2)	113.516(3)
volume (Å^3)	3255.1(4)	6752.6(12)	3273.5(3)	6756.6(13)
Z	1	2	1	2
$D_{calc.}$ (g/cm^3)	3.166	3.077	3.084	2.988
absorption coefficient (mm^{-1})	20.657	21.605	18.300	19.388
$F(000)$	2701	5402	2661	5273
R_{int}	0.0658	0.1183	0.0682	0.1229
θ range for data collection	2.704−27.579	2.052−26.504	2.642−27.541	1.394−26.470
completeness to θ_{max}	99.5%	98.9%	99.6%	99.3%
index ranges	$-17 \le h \le 17$, $-17 \le k \le 17$, $-23 \le l \le 23$	$-21 \le h \le 21$, $-24 \le k \le 24$, $-29 \le l \le 29$	$-17 \le h \le 17$, $-17 \le k \le 17$, $-23 \le l \le 23$	$-21 \le h \le 21$, $-24 \le k \le 24$, $-29 \le l \le 29$
reflections collected	61,300	115,664	61,676	118,159
unique reflections	14,981	27,727	15,041	27,775
data/restraints/parameters	14,981/366/658	27,727/678/1231	15,041/366/658	27,775/684/1243
goodness of fit on F^2	1.026	1.034	1.048	1.066
R_1[b] ($I > 2\sigma(I)$)	0.0375	0.0615	0.0377	0.0752
wR_2[c] (all data)	0.1061	0.1879	0.1100	0.2660

[a]Entries in brackets are the actual molecular formulae and weights of the compounds. [b]$R_1 = \sum||F_0| - |F_c||/\sum|F_0|$. [c]$wR_2 = [\sum w(F_0^2 - F_c^2)^2/\sum w(F_0^2)^2]^{1/2}$.

and 1,2,3,4,5-pentamethylcyclopentadiene (Cp*) were purchased from Sigma-Aldrich and used without further purification. The dimers $(Cp^*Ir^{III}Cl_2)_2$ and $(Cp^*Rh^{III}Cl_2)_2$ were synthesized according to the published procedures,[16] and their purity was confirmed by Fourier transform infrared (FTIR) and ^{1}H and ^{13}C NMR spectroscopy. The polyanion precursors $Na_{12}[Bi_2W_{22}O_{74}(OH)_2]\cdot 44H_2O$ and $K_{12}[Sb_2W_{22}O_{74}(OH)_2]\cdot 27H_2O$ were prepared according to the published procedures.[17] FTIR spectra were recorded on a Nicolet-Avatar 370 FTIR spectrophotometer using KBr pellets. Elemental analyses were done at ExxonMobil Chemicals Europe Inc., European Technology Center. Thermogravimetric analyses (TGAs) were performed on a SDT Q600 from TA Instruments under the flow of N_2 gas. The NMR spectra were recorded on a JEOL ECS 400 MHz spectrometer, using 5 mm tubes for ^{13}C and 10 mm tubes for ^{183}W NMR, with resonance frequencies of 100.71 and 16.69 MHz for ^{13}C and ^{183}W, respectively. The chemical shifts are reported with respect to the references $Si(CH_3)_4$ for ^{13}C and 1 M aqueous Na_2WO_4 for ^{183}W.

Synthesis of $Na_9K[\{RhC_{10}H_{15}\}_2Bi_2W_{20}O_{70}]\cdot 33H_2O$ (NaK-1). $(RhCp^*Cl_2)_2$ (0.009 g, 0.014 mmol) and $Na_{12}[Bi_2W_{22}O_{74}(OH)_2]\cdot 44H_2O$ (0.100 g, 0.014 mmol) were dissolved in 3 mL of 1 M aqueous sodium acetate (pH 6). The solution was heated at 70 °C for 30 min. After cooling down to room temperature, 100 μL of 1 M KCl were added to the solution. Red crystals of **NaK-1** started appearing overnight and were collected after 2 weeks (yield: 69 mg, 65%). FTIR (KBr pellet, 1650−400 cm^{-1}): $\bar{\nu}$ = 1628 (s), 1455 (sh), 1383 (sh), 942 (s), 797 (m), 755 (m), 643 (w) cm^{-1}. Elemental analysis: calculated (found): Na 3.2 (3.0), K 0.6 (0.7), Rh 3.2 (3.4), Bi 6.4 (6.8), W 56.3 (58.2). Cp*/POM ratio (based on TGA): 1.97.

Synthesis of $Na_{10}[\{IrC_{10}H_{15}\}_2Bi_2W_{20}O_{70}]\cdot 55H_2O$ (Na-2). $(IrCp^*Cl_2)_2$ (0.011 g, 0.014 mmol) and $Na_{12}[Bi_2W_{22}O_{74}(OH)_2]\cdot 44H_2O$ (0.10 g, 0.014 mmol) were dissolved in 3 mL of 1 M aqueous sodium acetate (pH 6). The solution was heated at 70 °C for 30 min and subsequently cooled down to room temperature. Red crystals started appearing overnight and were collected after 2 weeks (yield: 63 mg, 60%). FTIR (KBr pellet, 1650−400 cm^{-1}): $\bar{\nu}$ = 1627 (s), 1453 (sh), 1383 (sh), 941 (s), 794 (m), 744 (m), 643 (w) cm^{-1}. Elemental analysis: calculated (found): Na 3.2 (2.5), Ir 5.4 (5.2), Bi 5.9 (6.2), W 51.9 (53.0). Cp*/POM ratio (based on TGA): 1.99.

Synthesis of $Na_5K_5[\{RhC_{10}H_{15}\}_2Sb_2W_{20}O_{70}]\cdot 25H_2O$ (NaK-3). $(RhCp^*Cl_2)_2$ (0.009 g, 0.014 mmol) and $K_{12}[Sb_2W_{22}O_{74}(OH)_2]\cdot 27H_2O$ (0.087 g, 0.014 mmol) were added to 3 mL of 1 M aqueous sodium acetate (pH 6). The solution was stirred and heated at 70 °C for 30 min. After

https://doi.org/10.1021/acsomega.1c04707
ACS Omega 2021, 6, 34494−34500

cooling down to room temperature, 100 μL of 1 M KCl was added. Orange-red crystals started appearing overnight and were collected after 2 weeks (yield: 53 mg, 58%). FTIR (KBr pellet, 1650−400 cm^{-1}): $\bar{\upsilon}$ = 1631 (s), 1454 (w), 1378 (w), 945 (s), 846 (sh), 806 (w), 799 (m), 769 (w), 660 (s), 511 (w), 460 (w) cm^{-1}. Elemental analysis: calculated (found): K 3.1 (3.0), Na 1.8 (1.5), Rh 3.3 (3.4), Sb 3.9 (3.6), W 58.6 (59.6). Cp*/POM ratio (based on TGA): 1.93. The compound can also be synthesized using the sodium salt of the polyanion precursor.

Synthesis of $Na_{10}[\{IrC_{10}H_{15}\}_2Sb_2W_{20}O_{70}]\cdot 50H_2O$ (Na-4). $(IrCp^*Cl_2)_2$ (0.011 g, 0.014 mmol) and $K_{12}[Sb_2W_{22}O_{74}(OH)_2]\cdot 27H_2O$ (0.087 g, 0.014 mmol) were dissolved in 3 mL of 1 M aqueous sodium acetate (pH 6). The solution was heated at 70 °C for 30 min and then cooled down to room temperature. Orange-red crystals started appearing overnight and were collected after 2 weeks (yield: 33 mg, 31%). FTIR (KBr pellet, 1650−400 cm^{-1}): $\bar{\upsilon}$ = 1631 (s), 1565 (m), 1410 (w), 1384 (w), 946 (s), 860 (sh), 806 (s), 766 (w), 653 (s), 508 (w), 465 (w) cm^{-1}. Elemental analysis: calculated (found): Na 3.4 (2.1), Ir 5.6 (5.4), Sb 3.6 (3.7), W 53.9 (53.8). Cp*/POM ratio (based on TGA): 1.93. The compound can also be synthesized using the sodium salt of the polyanion precursor.

X-ray Diffraction (XRD). For each of the four compounds, a single crystal was mounted on a Hampton CryoLoop in light oil for data collection at 100 K. A Bruker D8 SMART APEX II CCD diffractometer with the kappa geometry and Mo-Kα radiation (a graphite monochromator, λ = 0.71073 Å) was used to perform indexing and data collection, whereas SAINT was used to perform data integration Routine Lorentz and polarization corrections were applied. Multiscan absorption corrections were performed using SADABS.[18] Direct methods (SHELXS97) successfully located the tungsten atoms, and successive Fourier syntheses (SHELXL2014) revealed the remaining atoms.[19] Refinements were performed with full-matrix least-squares against $|F^2|$ using all data. In the final refinement, all nondisordered heavy atoms (W, Rh, Ir, Sb, K, and Na) were refined anisotropically, whereas the disordered counter cations and all oxygen atoms were refined isotropically. No hydrogen atoms were included in the models. The formula units shown in the CIF files are based exclusively on the atoms detected by XRD on a single crystal, whereas the formula units shown in the paper are based on the true bulk composition of the compounds determined by elemental analysis. Small discrepancies are exclusively due to the exact number of disordered counter cations and crystal water molecules. Crystallographic data are summarized in Table 1. The CIF files are available online via the CCDC codes 2070002−2070005.

RESULTS AND DISCUSSION

The four polyanions $[\{RhCp^*\}_2Bi_2W_{20}O_{70}]^{10-}$ (**1**), $[\{IrCp^*\}_2Bi_2W_{20}O_{70}]^{10-}$ (**2**), $[\{RhCp^*\}_2Sb_2W_{20}O_{70}]^{10-}$ (**3**), and $[\{IrCp^*\}_2Sb_2W_{20}O_{70}]^{10-}$ (**4**) were synthesized by reacting the dimeric complexes $(MCp^*Cl_2)_2$ (M = Rh and Ir) in a 1:1 molar ratio with the heteropoly-22-tungstates $[X_2W_{22}O_{74}(OH)_2]^{12-}$ (X = Sb^{III} and Bi^{III}) in an aqueous medium at pH 6. Polyanions **1**−**4** are isostructural, comprising a dilacunary $[X_2W_{20}O_{70}]^{14-}$ unit with a Cp*M (M = Rh and Ir) entity grafted at each lacunary site via three M−O(W) bonds (the remaining coordination sphere of Rh/Ir is occupied by the Cp* ligand), leading to a structure with C_{2h} symmetry

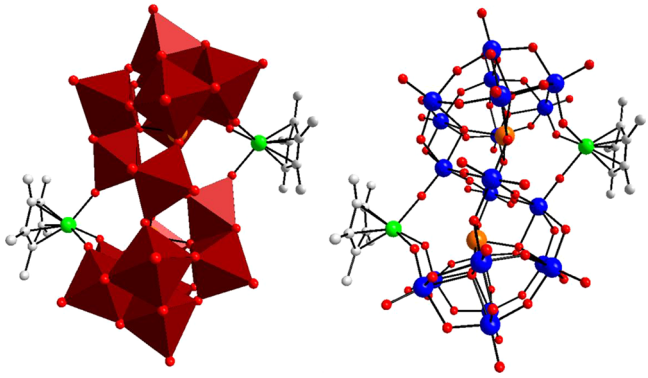

Figure 1. Polyhedral (left) and ball-and-stick (right) representation of polyanion **1**. Color code: Rh (green), W (blue), Bi (orange), O (red), C (gray), and WO_6 (dark red octahedra).

(Figure 1). It is relevant to mention that for each MCp* (M = Rh and Ir) unit, one M−O−W angle is ∼180°, whereas the other two are ∼140° each. The formation mechanism of **1**−**4** can be described as a substitution reaction of the 22-tungstate precursor, where two equivalent tungsten atoms with three terminal facial oxygens are replaced by organo-noble-metallic units. The coordination mode of the two MCp* (M = Rh and Ir) units in **1**−**4** is identical to that of arylruthenium(II) in $[(RuL)_2X_2W_{20}O_{70}]^{10-}$ (L = benzene and *p*-cymene; X = Sb^{III} and Bi^{III}).[20]

The number of crystal waters associated with each compound was determined by TGA on hydrated salts of **1**−**4**. The thermograms shown in Figure 2 exhibit two weight loss steps each. The first weight loss between room temperature and approximately 200 °C corresponds to the loss of crystal waters, whereas the second weight loss step after approximately 400 °C corresponds to the loss of the Cp* group attached to the noble metal atom Ir or Rh. The FTIR spectra of the hydrated salts of **1**−**4** are shown in Figure 3, and they show the expected bands. The broad band between 3000 and 3600 cm^{-1} is attributed to the O−H stretching vibration and the sharp band at 1650 cm^{-1} is attributed to the O−H bending vibration associated with the crystal water molecules. The C−H stretching vibrations of the Cp* methyl groups are assigned to the band at around 2900 cm^{-1}. The bands between 1350 and 1450 cm^{-1} can be assigned to the C−C stretching vibrations in Cp* and the rest of the peaks in the fingerprint region between 400 and 1000 cm^{-1} can be assigned to the W═O/W−O and Bi−O or Sb−O vibrations of the polyanions. The four IR spectra can be categorized into two sets, the Bi derivatives **1** and **2** and the Sb derivatives **3** and **4**.

Solution ^{183}W NMR studies were performed on **1**−**4** in order to study their solution stability (Figure 4). The ^{183}W NMR spectrum of **1** showed six singlets at −81.8, −83.4, −110.8, −118.1, −139.2, and −363.3 ppm, with relative intensities 2:2:2:2:1:1, respectively, in perfect agreement with the C_{2h} symmetry of the polyanion. The peak at −363.3 ppm, which is assigned to the W atom connected to the Rh atom via a linear oxo bridge, is a doublet due to $^{183}W-^{103}Rh$ coupling (^{103}Rh, S = 1/2, 100%) with a coupling constant of $^2J_{W\text{-}Rh}$ 3.0 Hz. On the other hand, the ^{183}W NMR spectrum of **3** showed only five peaks at −97.7, −106.4, −115.6, −144.5, and −361.0 ppm with relative intensities 2:2:4:1:1, respectively. The peak at −115.6 ppm integrates to a relative value of 4 but is actually composed of two overlapping peaks with an equal intensity of 2. This observation is fully consistent with the reported

https://doi.org/10.1021/acsomega.1c04707
ACS Omega 2021, 6, 34494−34500

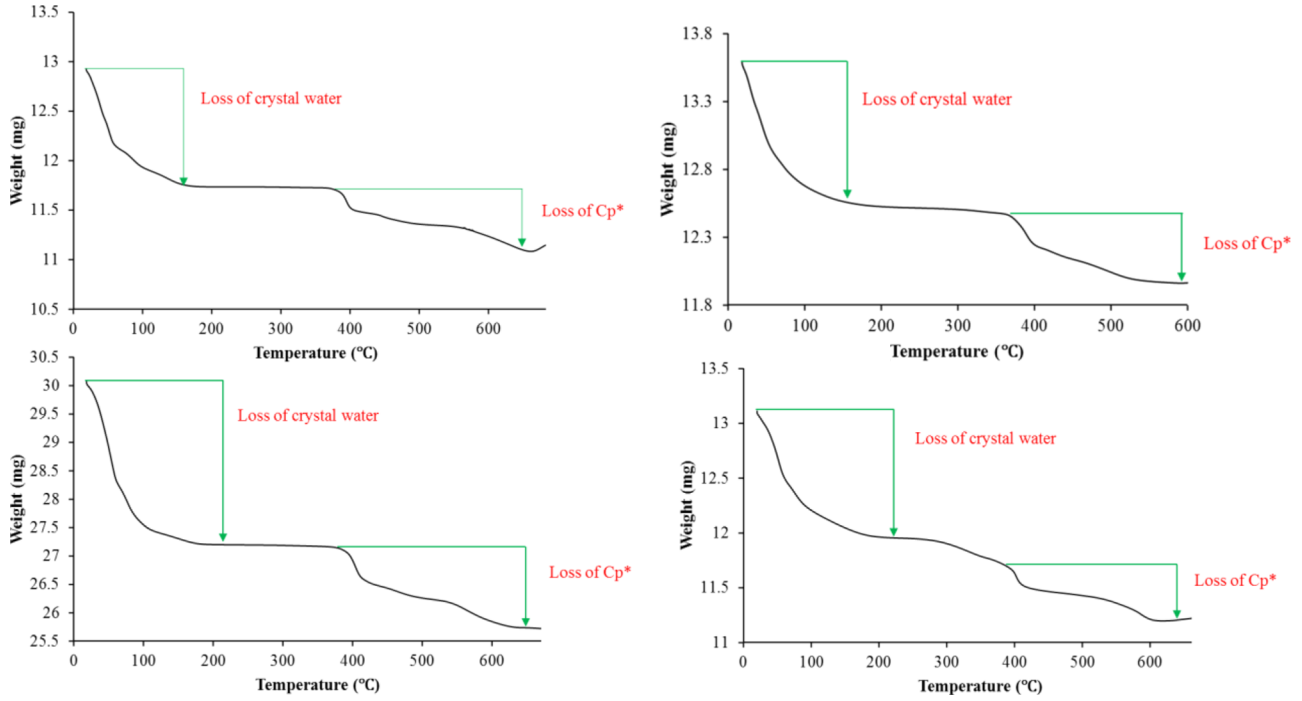

Figure 2. Thermograms of **NaK-1** (top left), **Na-2** (top right), **NaK-3** (bottom left), and **Na-4** (bottom right) from room temperature to 650 °C under a N_2 atmosphere.

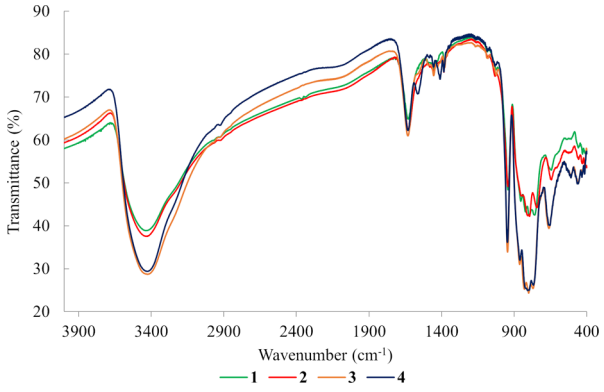

Figure 3. FTIR spectra of the hydrated salts of polyanions **1**−**4** (1 wt % in KBr pellets).

isostructural arylruthenium(II)-derivatives $[(RuL)_2Sb_2W_{20}O_{70}]^{10-}$ (L = benzene and *p*-cymene).[20,21] The peak at −361.0 ppm is a doublet due to $^{183}W-^{103}Rh$ coupling with a coupling constant of $^2J_{W\text{-}Rh}$ 3.0 Hz. The ^{183}W NMR spectrum of **2** showed the expected six peaks at −81.4, −87.9, −111.8, −119.3, −145.5, and −379.7 ppm with relative intensities of 2:2:2:2:1:1. Unlike the Rh-analogue **1**, the most upfield peak in the spectrum of **2** is a singlet due to the absence of any $S = 1/2$ nucleus for Ir. The ^{183}W NMR spectrum of **4** exhibited a six-line spectrum with peaks at −98.8, −117.3, −118.4, −121.0, −153.2, and −380.3 ppm. The peaks at −117.3 and −118.4 are closely spaced but can still be distinguished when focusing in this ppm region.

The ^{13}C NMR spectra of **1**−**4** in water are shown in Figure 5. All four polyanions exhibit the expected spectra with two ^{13}C peaks each. The upfield peak around 8 ppm corresponds to the five methyl carbons of the Cp* ligands and the more downfield peak around 94 ppm for the rhodium derivatives and 85 ppm for the iridium derivatives corresponds to the five aromatic carbon atoms constituting the five-membered Cp* ring. It is important to note that both Rh-containing polyanions **1** and **3** exhibit $^1J_{C\text{-}Rh}$ coupling between ^{103}Rh and the carbon atoms of the C_5 ring with coupling constants of 6.6 and 7.0 Hz, respectively. We also made extensive efforts to obtain ^{103}Rh NMR spectra for polyanions **1** and **3** but without success.

CONCLUSIONS

We have synthesized and structurally characterized the RhCp*- and IrCp*-containing polyanions $[\{RhCp^*\}_2Bi_2W_{20}O_{70}]^{10-}$ (**1**), $[\{IrCp^*\}_2Bi_2W_{20}O_{70}]^{10-}$ (**2**), $[\{RhCp^*\}_2Sb_2W_{20}O_{70}]^{10-}$ (**3**), and $[\{IrCp^*\}_2Sb_2W_{20}O_{70}]^{10-}$ (**4**), respectively. Polyanions **1**−**4** were synthesized by reacting $(MCp^*Cl_2)_2$ (M = Rh and Ir) in a 1:1 molar ratio with the heteropoly-22-tungstates $[X_2W_{22}O_{74}(OH)_2]^{12-}$ (X = Sb^{III} and Bi^{III}) in an aqueous medium at pH 6 and isolated as hydrated alkali salts. Polyanions **1**−**4** are isostructural, with two RhCp* or IrCp* groups grafted to dilacunary $[X_2W_{20}O_{70}]^{14-}$ polyanion fragments. All compounds were characterized in the solid state by single-crystal XRD, FTIR spectroscopy, and TGA and in solution by ^{183}W and ^{13}C NMR spectroscopy. The ^{183}W spectra of **1**−**4** showed the expected number of signals and relative intensities, although in **3**, two peaks are very closely spaced leading to an overlap. For **1** and **3**, the two-bond $^{183}W-^{103}Rh$ coupling in ^{183}W NMR could be observed. This is the ultimate evidence that the Rh atom remains attached to the POM framework in solution. Organorhodium and iridium-containing POMs are of interest for catalytic studies, which are currently ongoing in our laboratory.

ASSOCIATED CONTENT

Supporting Information

The Supporting Information is available free of charge at https://pubs.acs.org/doi/10.1021/acsomega.1c04707.

https://doi.org/10.1021/acsomega.1c04707
ACS Omega 2021, 6, 34494−34500

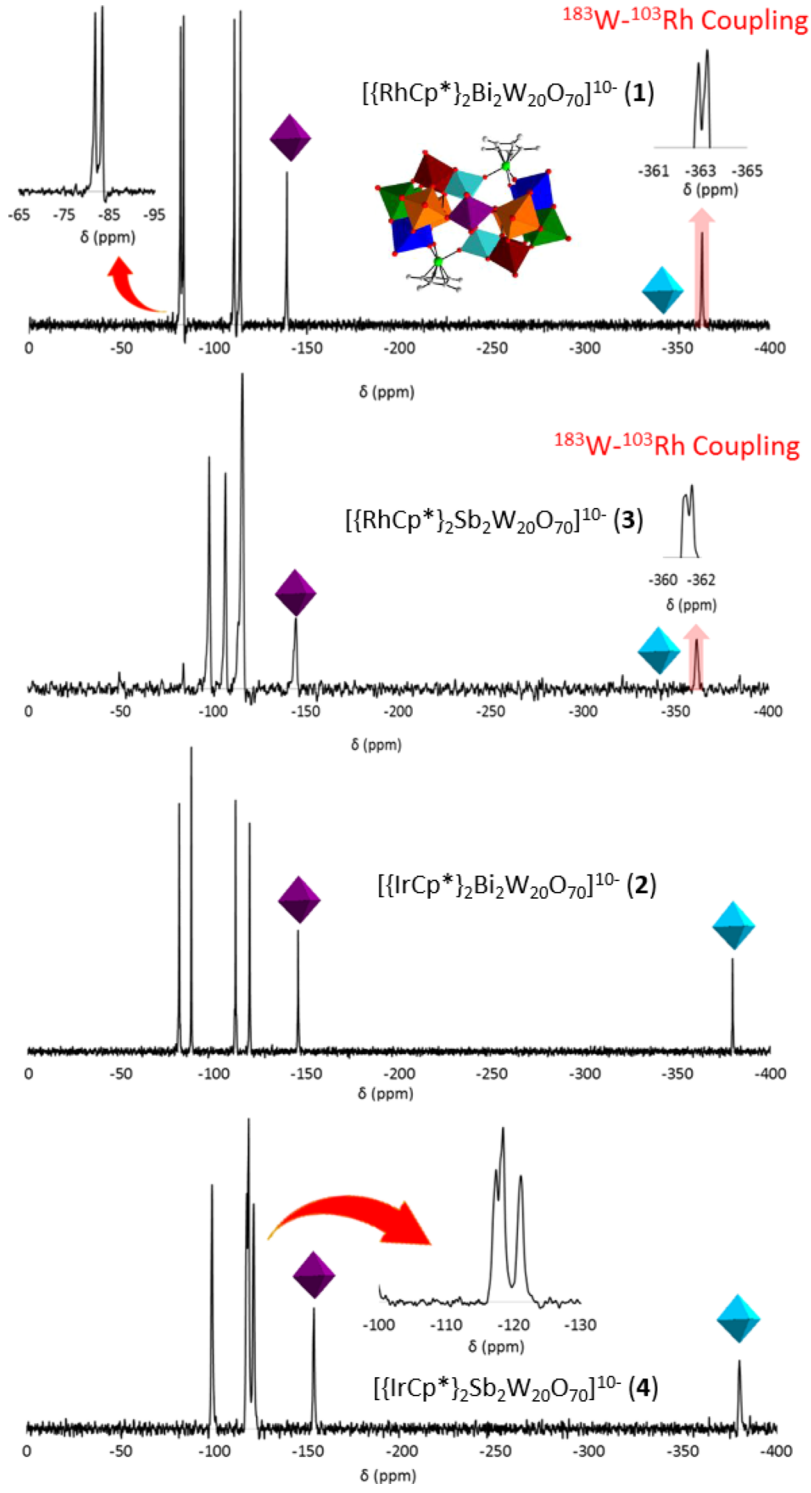

Figure 4. ^{183}W NMR spectra of polyanions **1**−**4** in H_2O/D_2O. The insets in the top two spectra show the doublets resulting from $^{2}J_{W\text{-}Rh}$ coupling. The polyhedral representation of the polyanion is representative for **1**−**4** and highlights the magnetically inequivalent tungsten centers in different colors.

Crystallographic data for Rh2Bi2W20 (CIF)
Crystallographic data for Ir2Bi2W20 (CIF)
Crystallographic data for Rh2Sb2W20 (CIF)
Crystallographic data for Ir2Sb2W20 (CIF)

Accession Codes

CCDC 2070002−2070005 contain the supplementary crystallographic data for this paper. These data can be obtained free of charge via www.ccdc.cam.ac.uk/data_request/cif, or by emailing data_request@ccdc.cam.ac.uk, or by contacting the Cambridge Crystallographic Data Centre, 12 Union Road, Cambridge CB2 1EZ, UK; fax: +44 1223 336033.

https://doi.org/10.1021/acsomega.1c04707
ACS Omega 2021, 6, 34494−34500

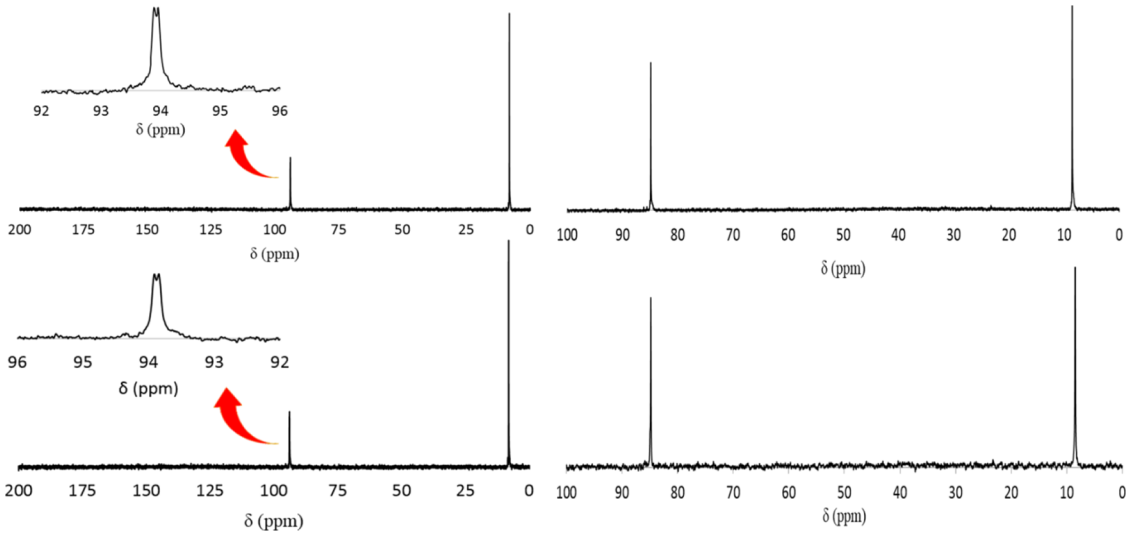

Figure 5. ^{13}C NMR spectra of **1** (top left), **2** (top right), **3** (bottom left), and **4** (bottom right) in H_2O/D_2O. The insets show the doublets resulting from $^{1}J_{C\text{-}Rh}$ coupling.

AUTHOR INFORMATION

Corresponding Author

Ulrich Kortz − *Department of Life Sciences and Chemistry, Jacobs University, 28759 Bremen, Germany;* orcid.org/0000-0002-5472-3058; Email: u.kortz@jacobs-university.de; Fax: (+49)421-200-3229

Authors

Ali S. Mougharbel − *Department of Life Sciences and Chemistry, Jacobs University, 28759 Bremen, Germany;* orcid.org/0000-0003-0108-3920

Sihana Ahmedi − *Department of Life Sciences and Chemistry, Jacobs University, 28759 Bremen, Germany*

Saurav Bhattacharya − *Department of Life Sciences and Chemistry, Jacobs University, 28759 Bremen, Germany;* orcid.org/0000-0002-3396-8312

Ananthu Rajan − *Department of Life Sciences and Chemistry, Jacobs University, 28759 Bremen, Germany;* orcid.org/0000-0001-9079-178X

Complete contact information is available at: https://pubs.acs.org/10.1021/acsomega.1c04707

Notes

The authors declare no competing financial interest.

ACKNOWLEDGMENTS

U.K. thanks the German Science Foundation (DFG, KO 2288/20-1), the CMST COST Action CM1203 (PoCheMoN), and Jacobs University for research support. We thank Dr. Wolfgang Baumann (LIKAT, Rostock) for helpful discussions and ^{103}Rh NMR measurements. Figure 1 was generated using Diamond, Version 3.2 (copyright Crystal Impact GbR).

DEDICATION

To the memory of Marcel Arndt (1995−2021).

REFERENCES

(1) Pope, M. T. *Heteropoly and isopoly oxometalates;* Springer Verlag, 1983.

(2) Pope, M. T.; Kortz, U. Polyoxometalates. In *Encyclopedia of Inorganic and Bioinorganic Chemistry*; John Wiley & Sons, 2012.

(3) (a) Izarova, N. V.; Pope, M. T.; Kortz, U. Noble Metals in Polyoxometalates. *Angew. Chem., Int. Ed.* **2012**, *51*, 9492−9510. (b) Yang, P.; Kortz, U. Discovery and Evolution of Polyoxopalladates. *Acc. Chem. Res.* **2018**, *51*, 1599−1608.

(4) (a) Besecker, C. J.; Day, V. W.; Klemperer, W. G.; Thompson, M. R. The $\{[(CH_3)_5C_5]Rh(cis\text{-}Nb_2W_4O_{19})\}^{2-}$ Isomers: Synthesis, Structure, and Dynamics. *J. Am. Chem. Soc.* **1984**, *106*, 4125−4136. (b) Finke, R. G.; Droege, M. W. Trisubstituted Heteropolytungstates as Soluble Metal Oxide Analogs. 1. The Preparation, Characterization, and Reactions of Organic Solvent Soluble Forms of the Silicon-Niobium Heteropolytungstates $Si_2W_{18}Nb_6O_{77}^{8-}$, $SiW_9Nb_3O_{40}^{7-}$, and the $SiW_9Nb_3O_{40}^{7-}$ Supported Organometallic Complex $[(C_5Me_5)Rh{\cdot}SiW_9Nb_3O_{40}]^{5-}$. *J. Am. Chem. Soc.* **1984**, *106*, 7274−7277.

(5) Nomiya, K.; Nozaki, C.; Kano, A.; Taguchi, T.; Ohsawa, K. Syntheses and Characterization of the Heptasodium Salt of the Keggin-Type Triniobium-Substituted Polyoxoanion $SiW_9Nb_3O_{40}^{7-}$ and the All-Sodium Salt of the Polyoxoanion-Supported Organometallic Complex $[(\eta^5\text{-}C_5Me_5)Rh{\cdot}SiW_9Nb_3O_{40}]^{5-}$. *J. Organomet. Chem.* **1997**, *533*, 153−159.

(6) Proust, A.; Gouzerh, P.; Robert, F. Organometallic Oxides: Lacunary Lindqvist-Type Polyanion-Supported Cyclopentadienylrhodium Complex Fragments. *Angew. Chem., Int. Ed.* **1993**, *32*, 115−116.

(7) Nomiya, K.; Hasegawa, T. Synthesis and Spectroscopic Characterization of a Dawson Trivanadium-Substituted Polyoxotungstate-Supported $\{(Cp^*Rh)_2\}^{4+}$ Complex; $(Bu^n_4N)_5[(Cp^*Rh)_2P_2W_{15}V_3O_{62}]$. *Chem. Lett.* **2000**, *29*, 410−411.

(8) Nomiya, K.; Sakai, Y.; Yamada, Y.; Hasegawa, T. Synthesis and Spectroscopic Characterization of a Keggin α-1,4,9-Trivanadium-Substituted Polyoxotungstate-Supported Cp^*Rh^{2+} Complex, $[(Cp^*Rh)(\alpha\text{-}1,4,9\text{-}PW_9V_3O_{40})]^{4-}$. *Dalton Trans.* **2001**, *52*−*56*, 52.

(9) Nomiya, K.; Sakai, Y.; Hasegawa, T. Synthesis and Spectroscopic Characterization of 1,2-Divanadium(v)-Substituted α-Dawson Polyoxotungstate-Based 1: 1-Type Cp^*Rh^{2+} Complex Showing Three Different Supporting Sites of the Cp^*Rh^{2+} Group. *Dalton Trans.* **2002**, *252*−*258*, 252.

(10) Nishikawa, K.; Kido, K.; Yoshida, J.; Nishioka, T.; Kinoshita, I.; Breedlove, B. K.; Hayashi, Y.; Uehara, A.; Isobe, K. Synthesis and Behavior in Solution of the Triple Cubane- and Windmill-Type Framework Isomers of an Organorhodium Tungsten Oxide Cluster $[(Cp^*Rh)_4W_4O_{16}]$. *Appl. Organomet. Chem.* **2003**, *17*, 446−448.

(11) Matsuki, Y.; Hoshino, T.; Takaku, S.; Matsunaga, S.; Nomiya, K. Synthesis and Molecular Structure of a Water-Soluble, Dimeric Tri-Titanium(IV)-Substituted Wells-Dawson Polyoxometalate Contain-

ing Two Bridging $(C_5Me_5)Rh^{2+}$ Groups. *Inorg. Chem.* **2015**, *54*, 11105−11113.
(12) Abramov, P. A.; Sokolov, M. N.; Virovets, A. V.; Floquet, S.; Haouas, M.; Taulelle, F.; Cadot, E.; Vicent, C.; Fedin, V. P. Grafting $\{Cp^*Rh\}^{2+}$ on the Surface of Nb and Ta Lindqvist-Type POM. *Dalton Trans.* **2015**, *44*, 2234−2239.
(13) Singh, V.; Ma, P.; Drew, M. G. B.; Niu, J.; Wang, J.; Jin, G.-X. Heterooctamolybdate-Based Clusters $H_3[(Cp^*Rh)_4PMo_8O_{32}]$ and $H_5[Na_2(Cp^*Ir)_4PMo_8O_{34}]$ and Derived Hybrid Nanomaterials with Efficient Electrocatalytic Hydrogen Evolution Reaction Activity. *Inorg. Chem.* **2017**, *56*, 12520−12528.
(14) Singh, V.; Ma, P.; Drew, M. G. B.; Wang, J.; Niu, J. A Comprehensive Approach Providing a New Synthetic Route for Bimetallic Electrocatalysts via isoPOMs $[M/Rh(Cp^*)_4W_8O_{32}]$ (M = Rh (1) and Ir (2)). *Dalton Trans.* **2018**, *47*, 13870−13879.
(15) Abramov, P. A.; Vicent, C.; Kompankov, N. B.; Gushchin, A. L.; Sokolov, M. N. Coordination of $\{C_5Me_5Ir\}^{2+}$ to $[M_6O_{19}]^{8-}$ (M = Nb, Ta) - Analogies and Differences between Rh and Ir, Nb and Ta. *Eur. J. Inorg. Chem.* **2016**, *2016*, 154−160.
(16) White, C.; Yates, A.; Maitlis, P. M.; Heinekey, D. M. (η^5-Pentamethylcyclopentadienyl)Rhodium and -Iridium Compounds. *Inorg. Synth.* **1992**, *29*, 229−234.
(17) (a) Loose, I.; Droste, E.; Bösing, M.; Pohlmann, H.; Dickman, M. H.; Rosu, C.; Pope, M. T.; Krebs, B. Heteropolymetalate Clusters of the Subvalent Main Group Elements Bi^{III} and Sb^{III}. *Inorg. Chem.* **1999**, *38*, 2688−2694. (b) Bösing, M.; Loose, I.; Pohlmann, H.; Krebs, B. New strategies for the generation of large heteropolymetalate clusters: The β-*B*-SbW_9 fragment as a multifunctional unit. *Chem. − Eur. J.* **1997**, *3*, 1232−1237.
(18) Sheldrick, G. *SADABS, Program for empirical X-ray absorption correction*; Bruker-Nonius: Madison, WI, 1990.
(19) Sheldrick, G. M. A short history of SHELX. *Acta Crystallogr., Sect. A: Found. Crystallogr.* **2008**, *64*, 112−122.
(20) Bi, L.-H.; Al-Kadamany, G.; Chubarova, E. V.; Dickman, M. H.; Chen, L.; Gopala, D. S.; Richards, R. M.; Keita, B.; Nadjo, L.; Jaensch, H.; Mathys, G.; Kortz, U. Organo-Ruthenium Supported Heteropolytungstates: Synthesis, Structure, Electrochemistry, and Oxidation Catalysis. *Inorg. Chem.* **2009**, *48*, 10068−10077.
(21) Laurencin, D.; Villanneau, R.; Herson, P.; Thouvenot, R.; Jeannin, Y.; Proust, A. A New Organometallic Heteropolytungstate Related to $[Sb_2W_{22}O_{74}(OH)_2]^{12-}$: Synthesis and Structural Characterisation of the bis-$\{Ru(p\text{-cymene})\}^{2+}$-Containing Anion $[Sb_2W_{20}O_{70}\{Ru(p\text{-cymene})\}_2]^{10-}$. *Chem. Commun.* **2005**, *44*, 5524−5526.

NOTE ADDED AFTER ASAP PUBLICATION

December 8, 2021. Additional changes were made to Table 1 presentation and data, and the corrected version was reposted on December 21, 2021.

https://doi.org/10.1021/acsomega.1c04707
ACS Omega 2021, 6, 34494−34500